Reflection extraction from sonic log waveforms using Karhunen-Loeve transform

Junxiao Li, Kris Innanen, Guo Tao and Laurence R. Lines

ABSTRACT

Sonic reflection logging, a recently developed borehole geophysical scheme, is in principle capable of providing a clear view of structures up to 40 m away from well site theoretically. Under acoustic well logging conditions, reflected wave signals used in sonic reflection logging are generally lost in the full waveform records, hidden by the dominant direct waves (direct P- and S- waves, and the Stoneley wave). It is critical, therefore, to effectively extract the reflection signals from the acoustic full waveforms in acoustic reflection well logging data processing. The Karhunen-Loeve (KL) transformations combined with a band limiting filter is used to extract reflections of interest out of dominant direct waves. Based on energy difference of each wave component, the direct Stoneley wave, S wave and P wave are to be eliminated separately from high to low energy component. Therefore, the extracted reflections can then be used in migration so as to get a clear image of the structures outside borehole.

INTRODUCTION

Sonic logging was first proposed to measure the speed of sound in a short interval of rock traversed in a wellbore by using a transmitter and two receivers (Marguerite, 1940). However, it was not specifically used to measure P- and S-wave velocities until the 1960s (Kokesh et al., 1965). Usually, a recorded waveform generated by the transmitter consists of not only refracted P- and S-wave, but also the Pseudo Rayleigh wave and the Stoneley wave (Cheng and Toksöz, 1981). Compared with body waves (P- and S-waves) from surface seismic data, sonic P- and S-waves in the borehole (also called head waves) usually exist as higher-frequency and shorter-wavelength. Pseudo Rayleigh waves, which only exist under the circumstance when the formation shear velocity is greater than the fluid velocity in the borehole (Tang and Cheng, 2004), is a surface wave characterized by elliptical particle motion and transmitted along the formation fluid interface. The Stoneley wave, which shows dispersive characteristics, is always slower than the head waves and tends to dominate the full recorded waveform.

Conventionally, sonic logging technology uses direct sonic arrivals (P- and S-waves) to calculate formation P- and S- wave velocities (Kimball and Marzetta, 1984). It is also used to determine in suit attenuation from full waveform acoustic logs (Cheng et al., 1982). In 1989, Hornby discovered the influence of formation permeability on Stoneley wave slowness and proposed a method for determining formation permeability using these waves (Hornby et al., 1989).

Recently, secondary arrivals (reflections from structures outside the borehole) have increasingly been used for characterizing geological structures away from a wellbore (Hornby, 1989b; Coates and Schoenberg, 1995; Chabot et al., 2001). This idea, however, was originated almost 30 years ago when Hornby (Hornby, 1989a) presented data processing and

imaging methods involving secondary compression arrivals to form an image of the formation structures, in which a frequency-wavenumber transform is used for elimination of the direct arrivals and other sources of noise. However, the reflected waves are difficult to discover amongst the much higher amplitude head waves. Extraction of reflections is a key technological hurdle to practical use of sonic full waveforms. A combination of FK and median filtering techniques has been tested for reflection extraction in single-well imaging with acoustic reflection survey (Li et al., 2002). The median filter is used to remove direct waves, and then the FK filter is applied to separate downgoing and upgoing reflections. Tang (2004), and Zheng et al. (2005) used the parametric prediction method to extract reflection waves from waveforms. When this did not achieve satisfactory results, a geometric spreading factor was introduced to modify the parametric prediction method (Bing et al., 2011). Independently, blind source separation (BSS) was introduced to borehole geophysics (Li et al., 2014a) to extract reflections. However, amplitude information is missed using BSS, which makes it difficult to obtain ideal reflections by simply deducting the extracted head waves by applying BSS from the full waveforms.

The Karhunen-Loeve (KL) transformation has been widely used in data analysis such as imaging compression (Ahmed and Rao, 2012) and image coding (Andrews and Patterson III, 1976). The KL transformation has also been used in seismic exploration for signal-to-noise improvement (Hermon and Mace, 1978), diffraction separation from reflections (Yedlin et al., 1987). Hsu (1990) used the KL transformation to sonic logging waveforms to extract direct waves. In his paper, a threshold detection scheme is first applied before using KL transformation to exclude the unwanted signals. The KL transformation is applied in acoustic reflection well logging to extract reflections from direct waves. However, when extracting the reflection signals, based on the energy difference (the direct waves have higher energy than do the reflections), the unwanted signals can be eliminated by choosing a wide processing window, where a precise threshold is not necessary needed. When fractures exist around the borehole, a Stoneley signal will generate the so-called reflection Stoneley when traveling through fractures (Paillet and White, 1982; Hornby et al., 1989). Therefore, for the Stoneley wave elimination in field data, a band limit filter is instead used, because the reflected Stoneley can not be mitigated by KL transformation.

KARHUNEN-LOEVE(KL) TRANSFORM

The typical sonic log can be considered as a N-dimensional vector $\mathbf{X} = (X_1, X_2, \cdot \cdot \cdot, X_n)$, each vector X_i can be treated as a recorded waveform at specific depth. Therefore, N denotes the total number of recorded waveforms. The mean value of this N-dimensional vector can be described as,

$$\mu_X = \frac{1}{N}\sum_{i=1}^{N} X_i \tag{1}$$

Its covariance matrix thus can be written as,

$$C_X = E\{(X_i - \mu_X)(X_i - \mu_X)^T\} = \frac{1}{N}\sum_{i=1}^{N}(X_i - \mu_X)(X_i - \mu_X)^T \tag{2}$$

where, E denotes the mathematical expectation and T denotes the transpose of the matrix.

Assume $\lambda_i(i = 1, 2, \cdots, N)$ being the eigenvalue of the covariance matrix with its correspondent eigenvector $e_i(i = 1, 2, \cdots, N)$, therefore, we have an orthogonal matrix of **A**, where **A** can be described as,

$$\mathbf{A} = \begin{bmatrix} e_1^T \\ e_2^T \\ e_3^T \\ \cdots \\ e_N^T \end{bmatrix} \tag{3}$$

for $\lambda_1 >= \lambda_2 >= \lambda_3 >= \cdots >= \lambda_N$. Therefore, we have,

$$\mathbf{Y} = \mathbf{A}(\mathbf{X} - \mu_X)$$

$$Y_i = e_i^T(X_i - \mu_X) \tag{4}$$

Y_i denotes each component of $\mathbf{Y}$. Because **A**is an orthogonal matrix ($\mathbf{A}^- = \mathbf{A}^T$), the N-dimensional vector **X** can be stated as,

$$\mathbf{X} = \mathbf{A}^T\mathbf{Y} + \mu_X \tag{5}$$

Now, let's consider the first k largest eigenvectors,

$$\mathbf{A} = \begin{bmatrix} e_1^T \\ e_2^T \\ e_3^T \\ \cdots \\ e_k^T \end{bmatrix} \tag{6}$$

for $\lambda_1 >= \lambda_2 >= \lambda_3 >= \cdots >= \lambda_k, k < N$.

Then we have an approximate matrix of **A**,

$$\hat{\mathbf{X}} = A_k\mathbf{Y} + \mu_X$$

$$\hat{X}_i = e_i^T Y_i + \mu_X \tag{7}$$

where,$\hat{X}_i$ denotes each component of $\hat{\mathbf{X}}$. The mean square error between $\mathbf{X}$ and $\hat{\mathbf{X}}$ becomes,

$$\varepsilon(k) = E\{(\mathbf{X} - \hat{\mathbf{X}})^T(\mathbf{X} - \hat{\mathbf{X}})\} = \frac{1}{N-k}\sum_{i=k+1}^{N} X_i X_i^T \tag{8}$$

In geophysical signal analysis, the received signal is usually considered as a zero mean value (Saggaf and Robinson, 2000), which means μ_X is equal to 0. Therefore, the mean square error will be minimized when

$$C_X e_i = \lambda_i e_i, \qquad i = k+1, \cdots, N \tag{9}$$

Therefore, we have

$$\varepsilon(k) = \sum_{i=k+1}^{N} \lambda_i \tag{10}$$

The approximated term in equation (7) thus can be used to reconstruct the original signal if and only if the mean square error approximates 0. This means if the first k number of dominant eigenvectors are used to reconstruct the original information, the dominant energy can be reconstructed by this method, which is called KL transformation. In acoustic reflection logging, most of the energy comes from the direct P- and S- waves, and the Stoneley waves, which can be extracted from the full waveforms by means of KL transformation. Whereas the residuals excluding the direct waves should be the reflections, which can be further used in acoustic reflection logging.

WAVE SEPARATION USING KL TRANSFORMATION

In order to demonstrate the reflection extraction from sonic logging by KL transformation. A synthetic data simulated by finite difference method is used. The model (shown in Figure 1) is a fluid filled borehole model with a fault like interface lies on the one side of the borehole with a dip of 45 degrees. The model is 15 m high by 10 m long, in which the diameter of the borehole is 0.2 m. The borehole located at the lateral depth of 1m, is filled with water, shown in blue color. The formation in red stands for medium I and that in yellow is medium II. The acoustic reflection logging tool is designed to have a source-receiver spacing of 3 m, and a total number of thirteen receivers separated with an interval of 0.15 m. The borehole and formation parameters are shown in Table 1.

Table 1. Parameters of fault-like model outside the borehole

	c_{11}	c_{13}	c_{33}	c_{44}	$\rho(g/cm^3)$
Yellow	23.87	9.79	15.33	2.77	2.5
Borehole	2.25	2.25	2.25	0	1
Red	40	13.55	40	13.225	2.5

Firstly, we move the source point from depth of 2 m to 10.85 m with altogether 60 shots, whose depth interval is 0.15 m. A 2D FD numerical modeling is used to acquire the acoustic

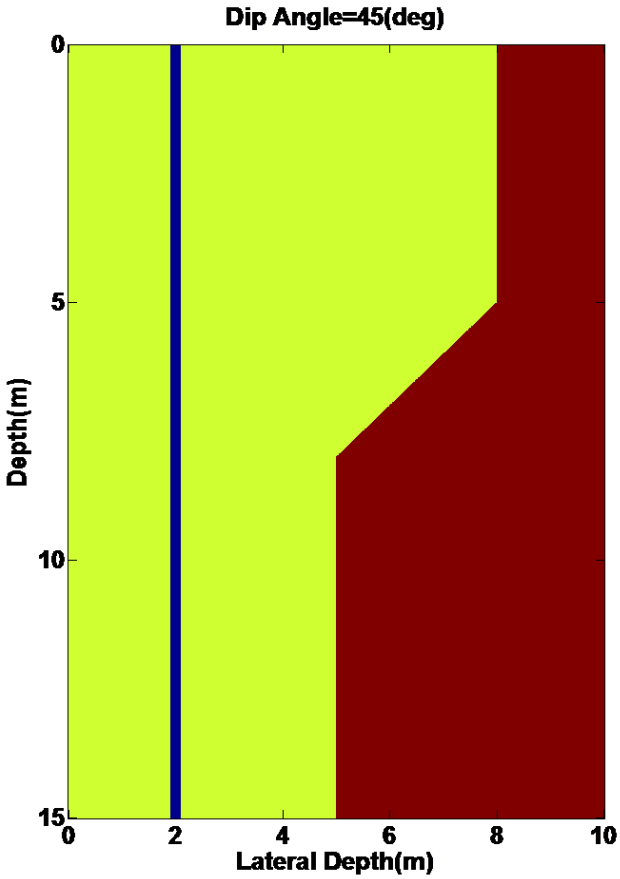

FIG. 1. Synthetic model simulated by finite difference method. Blue area represents a borehole filled with water. Yellow and red areas are two formations with different properties shown in Table 1.

array full waveform for each source point. Figure 2 (left) shows the received full waveform when the dip angle is 45 degrees. The total recording time is 3 ms. After elimination of direct waves, the refection signals can be acquired, shown in Figure 2 (Right). As shown in Figure 2 (Left), because of the slow formation outside the borehole, the first arrived signal is leaky P wave signal; the water wave (whose velocity is about 1500 m/s) signal propagating in the borehole fluid is behind the P wave signal; signal behind the water wave is Stoneley wave. There is no shear wave signal in slow formation. The theoretical reflections can be simply obtained by subtracting the full waveforms with direct arrivals (P wave and Stoneley wave).

As has been discussed in the last section that KL transformation is also known as principal-component analysis. If KL transformation is applied at a wide range from 0 ms to 1.5 ms, theoretically, the principal component should be the Stoneley wave who has the highest amplitude. Figure 3 shows the four dominant normalized eigenvectors of covariance matrix calculated from the selected range of full waveforms. Compared the take-off time of each event shown in Figure 2 (Left), the first dominant eigenvector consists not only

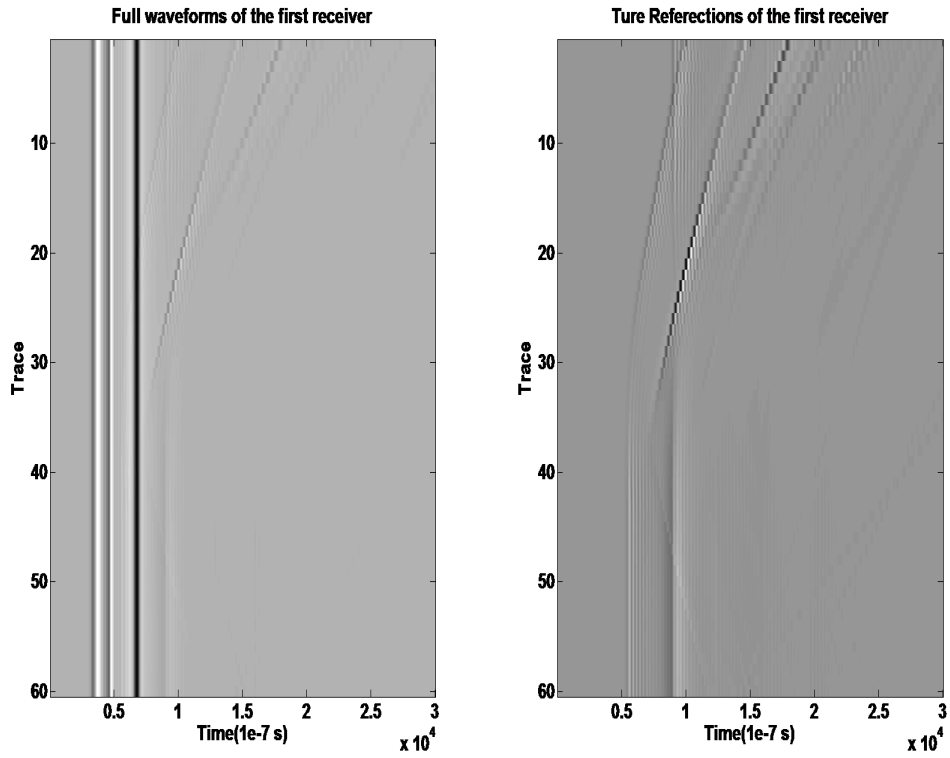

FIG. 2. Received full waveform when the dip angle is 45 degree (Left) and theoretical refection signals after the direct signals have been removed (Right).

of the Stoneley component, but also of the water wave component as well. The eigenvalue of the first dominant eigenvector is 0.9949, which shows 99 percent of total energy comes from the first eigenvector.

As a result, first principal component can be reconstructed by only using the first dominant eigenvector shown in Figure 4 (Left) and Figure 4 (Right) shows the covariance residuals after the first principal component is eliminated. The reflected waves emerge as a subsequence following the new principal component in Figure 4 (Right).

Following the water wave and Stoneley wave extraction, the head P wave becomes the dominant event. A same time window from 0 ms to 1.5 ms is applied to calculate covariance matrix of the waveform and its four dominant eigenvectors are then show in Figure 5(Left).

The first eigenvector has a eigenvalue of 0.9976, which shows most of the P wave energy has been converged into the first dominant eigenvector. Therefore, only the first dominant eigenvector is used to reconstruct the P wave, shown in Figure 6(Left). Figure 6 (Right) shows the residuals after the P wave component has been removed, which actually is the extracted reflections after eliminating the direct P wave, water wave and Stoneley wave respectively. Compared with the theoretical reflections shown in Figure 2 (Right), almost all the reflection details have been revealed. To make a comparison, the result of reflections extracted using multi-scale slowness-time-coherence (MSTC) (Tao et al., 2008)

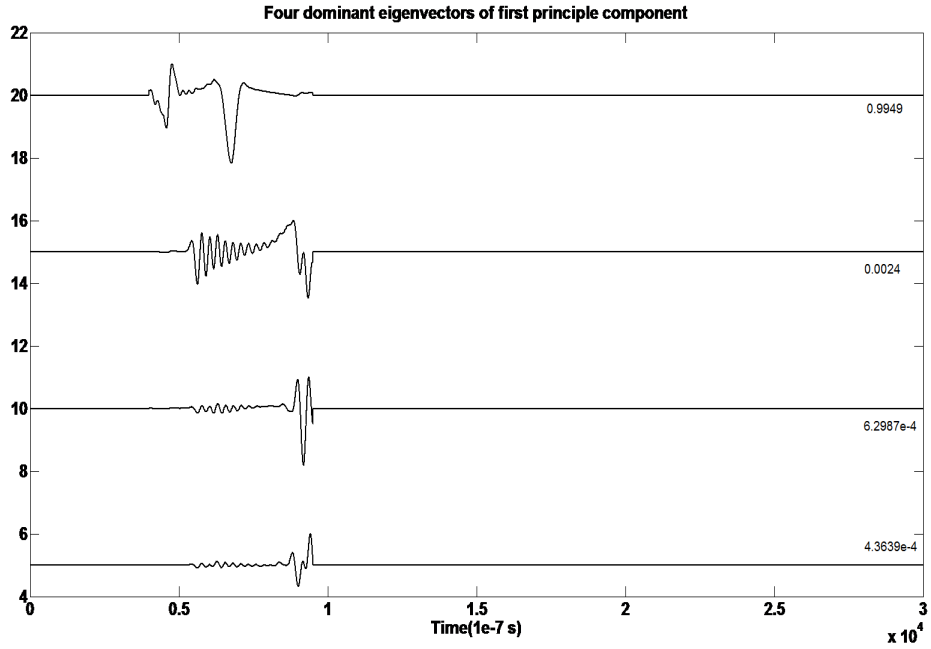

FIG. 3. Four dominant normalized eigenvectors of covariance matrix calculated from the selected range of full waveforms. The eigenvalue of each eigenvector is also shown.

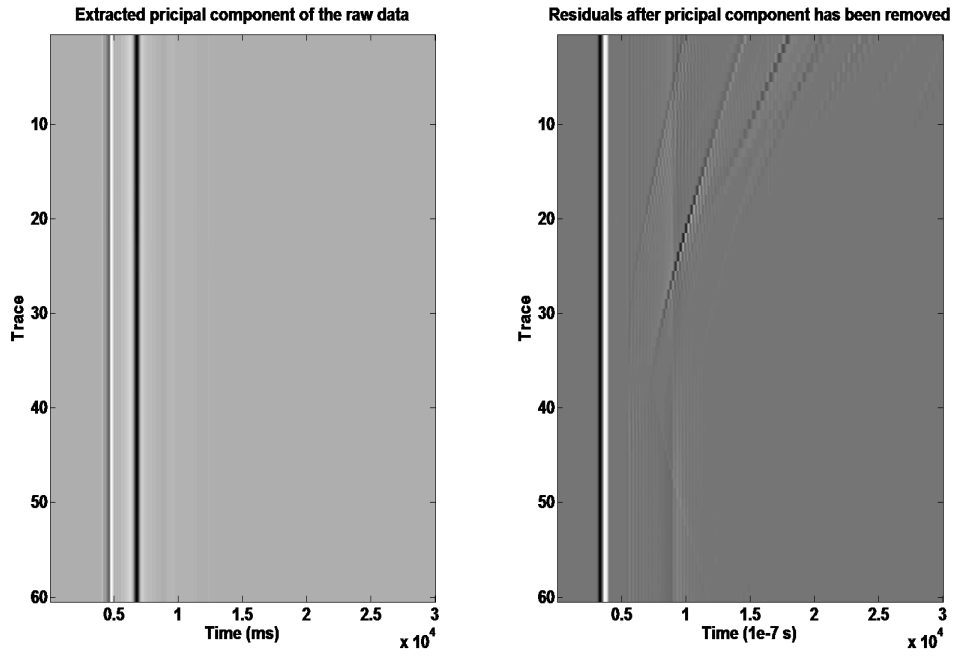

FIG. 4. First principal component of the raw data (Left) and residuals after principal component has been removed (Right).

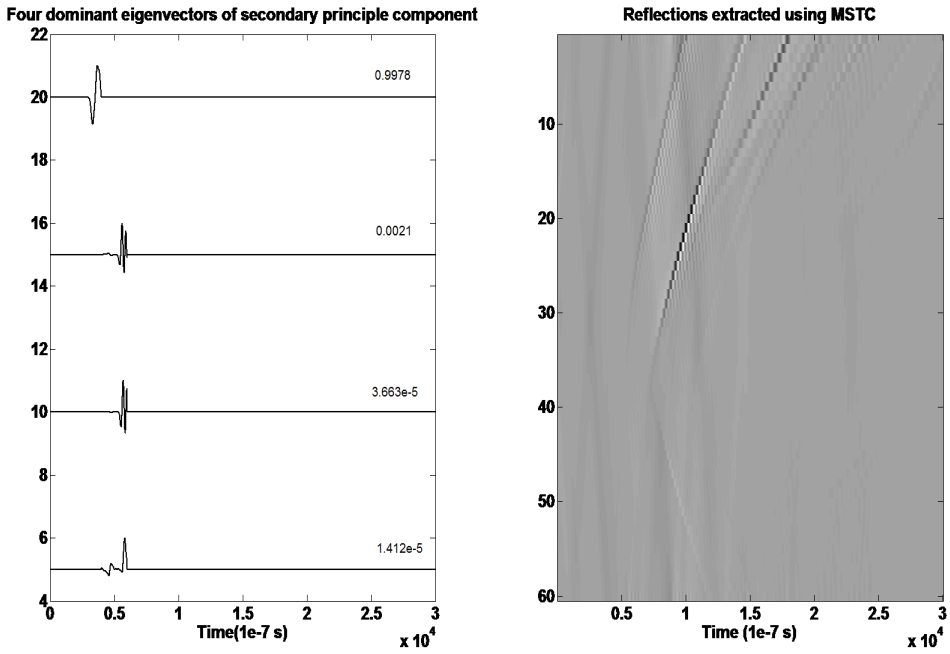

FIG. 5. Four dominant eigenvectors of the residuals after principal component is removed (Left) and reflections extracted using MSTC (Right).

is also displayed in Figure 5 (Right), where some details of the reflection signals are missing and low frequency noises appear during the whole recording time.

Laboratory data example

In this section, the laboratory data is acquired in a specially designed large water tank by the remote exploration acoustic reflection imaging instrument. The reflector in the water tank is a steel pad placed at an angle of 20 degrees and distanced 3 m away from the tool. The depth interval is 0.1524 m and the distance between the source to the first receiver is 5.3 m. The received full waveforms by the first receiver is shown in Figure 7 (Left), where the event at around 6 ms whose speed is about 900 m/s has the strongest energy, which should be the principal component that we don't want. The P head wave event is at about 4 ms with a velocity of roughly 1400 m/s. There is also some unwanted low frequency noise at the beginning of the waveform. Figure 7 (Right) shows the reflection extraction result by using MSTC, where the reflections from the steel pad emerges yet accompanied by some remnants both from direct P wave and Stoneley wave components scattering along the depth interval.

Figure 8 (Left) shows the principal component extracted by the KL transformation. Figure 8 (Right) shows the residuals after the principal component has been removed. The feeble reflection of the steel pad emerges in the full waveforms where the low frequency noise at the beginning and the P head wave components take dominant roles. Figure 9 (Left) shows the secondary component extracted by the KL transformation after the low frequency noise is removed by a high bandpass filter. Figure 9 (Right) shows the reflection signals

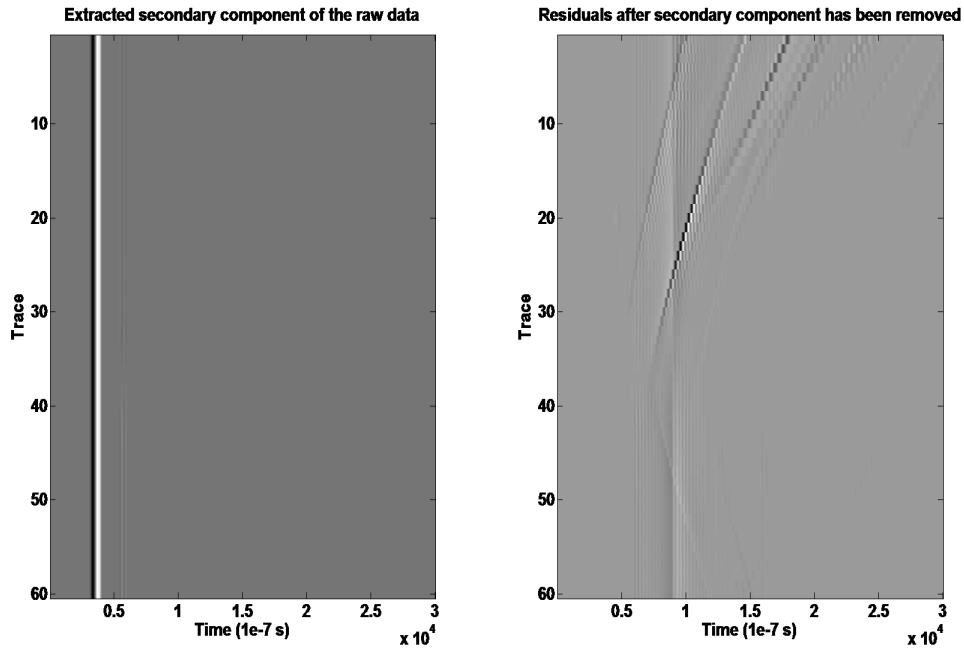

FIG. 6. Reconstruct the P wave component extracted using the first eigenvector (Left) and residuals after secondary component has been removed (Right).

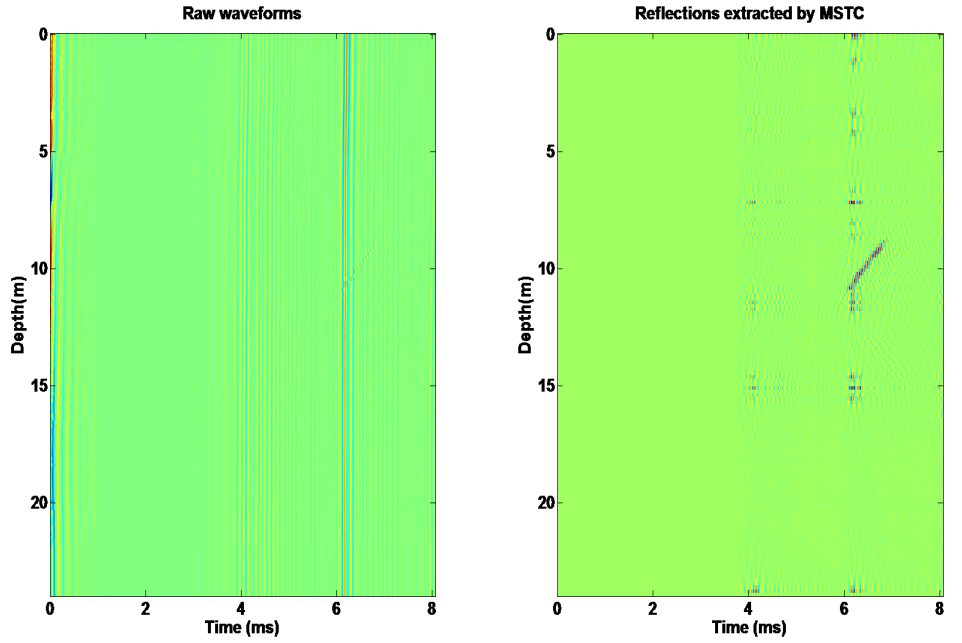

FIG. 7. Received full waveform of the water tank data (Left) and refection signals using MSTC (Right).

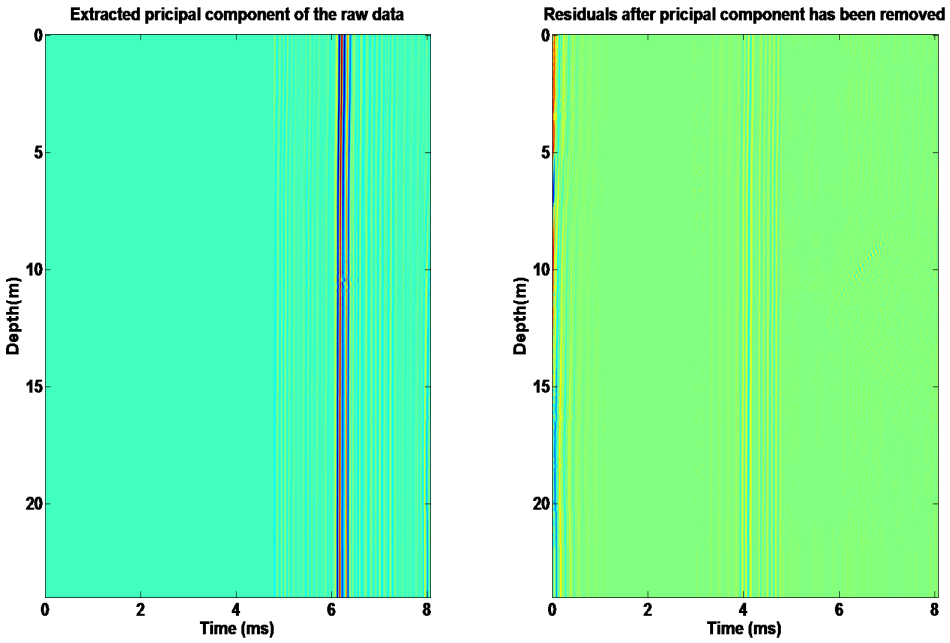

FIG. 8. First principal component of the raw data (Left) and residuals after principal component has been removed (Right).

from the steel pad after the secondary component has been removed. Compared with the result obtained using MSTC, the main difference is there is no scattered residual energy left. The acquired reflections by KL transformations can now be used in the migration step. The borehole reverse time migration (RTM) (Li et al., 2014b) is applied, in which the staggered grid finite difference method is used for the forward and backward simulation and the hybrid perfectly matched layer (H-PML) (Zhang et al., 2014) is used for the absorbing layers. The imaging result is shown in Figure 10 (Left), as can be seen in the imaging result, the steel pad is clearly shown at an angle of 20 degrees and a distance of 3 m away from the borehole, and the shape of the pad can be clearly observed. To make a comparison, the reflections obtained by the MSTC is also displayed in Figure 10 (Right), where, however, the imaging result suffers inevitably from the influence of the scattered remains.

Filed data example

The field data used in this paper was acquired by an acoustic reflection imaging instrument from East Asia. The source to the first receiver distance of this tool is 3.6576 m with a receiver interval of 0.1524 m. The altogether 8 evenly spaced receivers record waveforms transmitted from the source with a recording sampling rate of 12 us. Figure 11 (Left) shows a set of single-receiver waveforms received by the first receiver from a depth range of 70 m (450 waveforms). According to KL transformation, the principal energy (Stoneley wave component) should be removed first. As a result, Figure 11 (Middle) shows the residuals after the Stoneley direct wave is removed, whereas the Stoneley reflections with a large range of recording time between trace 300 to 350 emerges. And the echo of the Stoneley energy around 6000 ms is another problem for the reflection extraction. Therefore, the

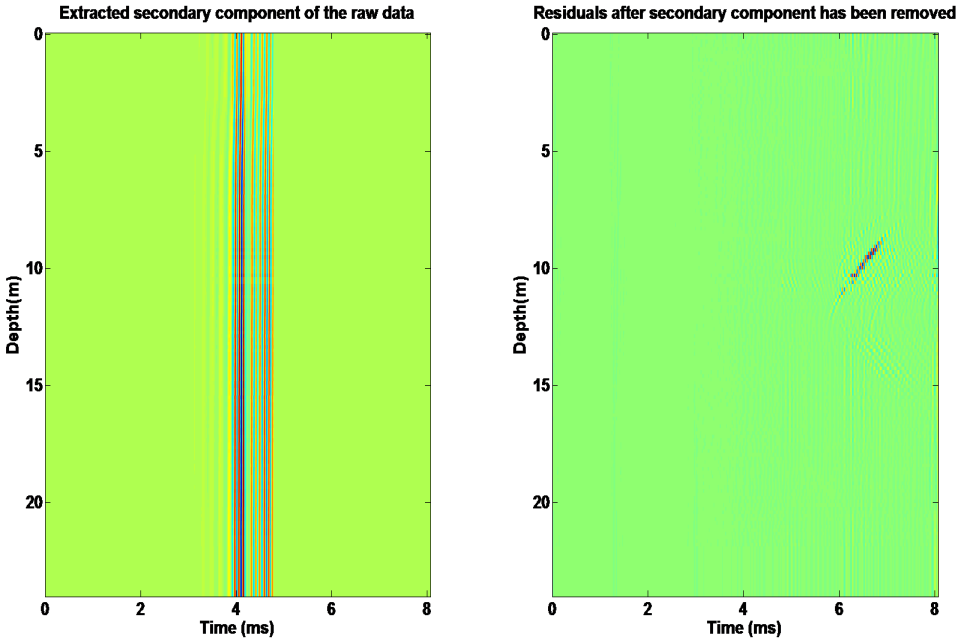

FIG. 9. Reconstruct the P wave component extracted using the first eigenvector (Left) and residuals after secondary component has been removed (Right).

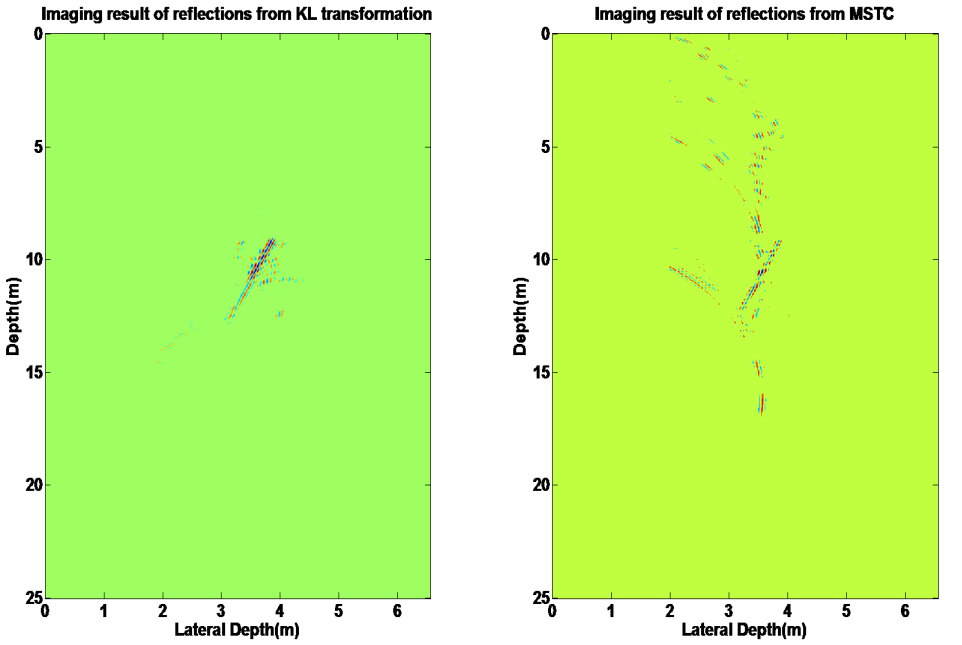

FIG. 10. Imaging result of reflections from KL transformation (Left) and result of reflection from MSTC (Right).

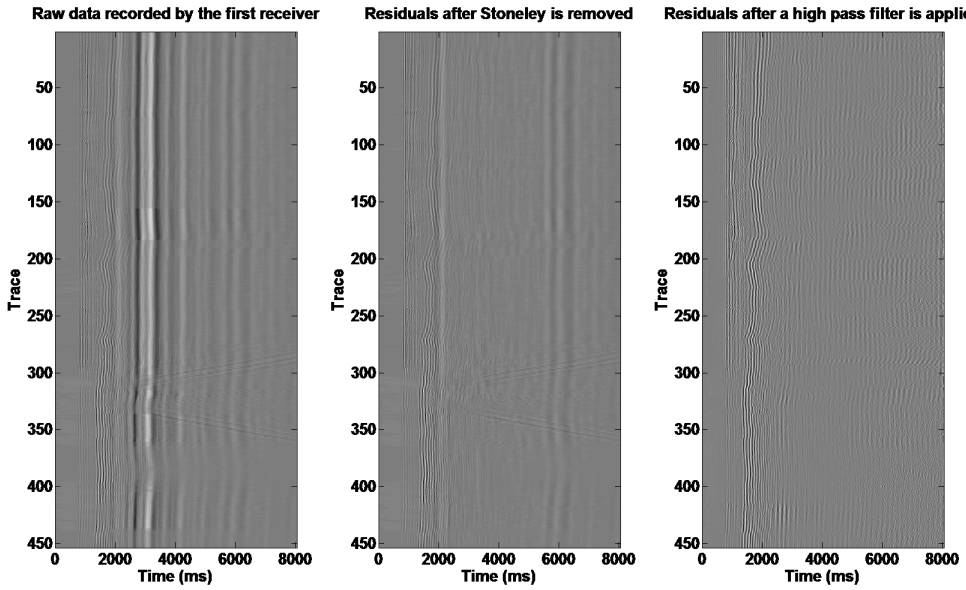

FIG. 11. The raw waveforms recorded by a receiver (Left); the residuals after the Stoneley direct wave is removed (Middle) and results after the Stoneley energy has been removed by a high-pass filter (Right).

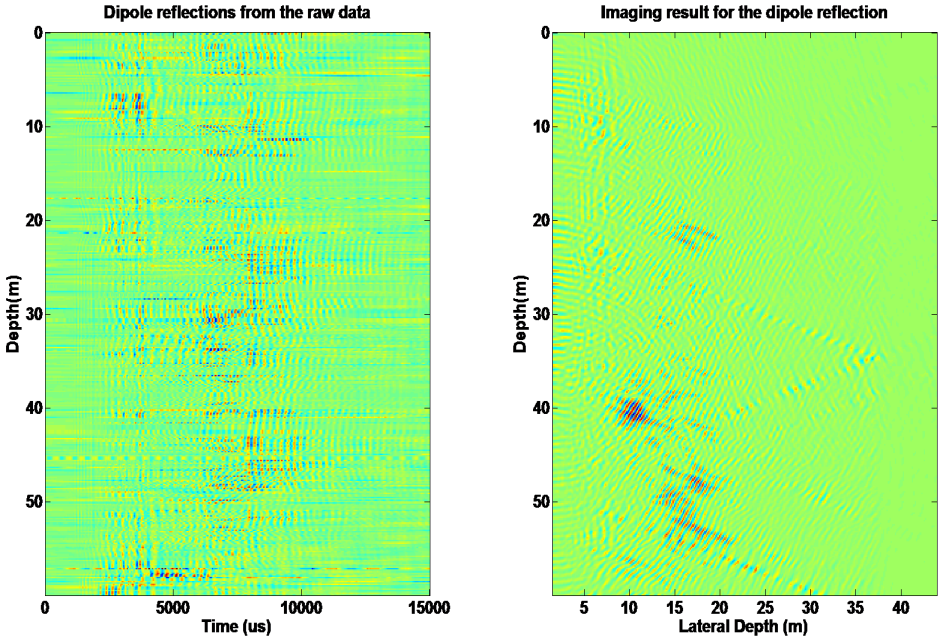

FIG. 12. Reflections acquired from the dipole recorded signals (Left); the imaging result for the dipole reflections (Right).

Stoneley energy should be removed by a high pass filter based on the frequency band difference between Stoneley wave and P- and S-waves. Figure 11 (Right) shows the results after the Stoneley wave has been successfully removed.

In order to get an imaging result with a wide lateral detection depth. The dipole reflections acquired from the dipole recorded signals shown in Figure 12 (Left) are used in migration. Figure 12 (Right) shows the imaging result for the dipole reflections. The reflectors can be clearly seen at about 10 m to 20 m outside of borehole. As can also be seen, the lateral depth for dipole signals can reach up to 40 m away from borehole.

CONCLUSIONS

The KL transformation is applied in this paper to separate reflections away from direct signals in acoustic reflection well logging data. Based on energy difference of each signal component, the direct P- and S waves as well as the Stoneley wave can be efficiently removed. Comparisons with MSTC method both from synthetic and laboratory data show KL transformation is capable of providing much more precise reflection signals. For the field data, a high pass filter is applied first to mitigate Stoneley direct and reflect signals, given the reason that the KL transformation can not remove the Stoneley reflections.

ACKNOWLEDGMENTS

The authors thank the sponsors of CREWES for continued support. This work was funded by CREWES industrial sponsors and NSERC (Natural Science and Engineering Research Council of Canada) through the grant CRDPJ 461179-13. Author 1 was also supported by SEG scholarship and Shell.

REFERENCES

Ahmed, N., and Rao, K. R., 2012, Orthogonal transforms for digital signal processing: Springer Science & Business Media.

Andrews, H. C., and Patterson III, C. L., 1976, Singular value decomposition (svd) image coding: Communications, IEEE Transactions on, **24**, No. 4, 425–432.

Bing, W., Guo, T., Hua, W., and Bolei, T., 2011, Extracting near-borehole p and s reflections from array sonic logging data: Journal of Geophysics and Engineering, **8**, No. 2, 308.

Chabot, L., Henley, D. C., Brown, R. J., Bancroft, J. et al., 2001, Single-well imaging using the full waveform of an acoustic sonic, *in* 2001 SEG Annual Meeting, Society of Exploration Geophysicists.

Cheng, C. H., and Toksöz, M. N., 1981, Elastic wave propagation in a fluid-filled borehole and synthetic acoustic logs: Geophysics, **46**, No. 7, 1042–1053.

Cheng, C. H., Toksöz, M. N., and Willis, M. E., 1982, Determination of in situ attenuation from full waveform acoustic logs: Journal of Geophysical Research: Solid Earth (1978–2012), **87**, No. B7, 5477–5484.

Coates, R. T., and Schoenberg, M., 1995, Finite-difference modeling of faults and fractures: Geophysics, **60**, No. 5, 1514–1526.

Hornby, B., Johnson, D., Winkler, K., and Plumb, R., 1989, Fracture evaluation using reflected stoneley-wave arrivals: Geophysics, **54**, No. 10, 1274–1288.

Hornby, B. E., 1989a, Imaging of near-borehole structure using full-waveform sonic data: Geophysics, **54**, No. 6, 747–757.

Hornby, B. E., 1989b, Method for determining formation permeability by comparing measured tube waves with formation and borehole parameters, uS Patent 4,797,859.

Hsu, K., 1990, Wave separation and feature extraction of acoustic well-logging waveforms using karhunen-loeve transformation: Geophysics, **55**, No. 2, 176–184.

Kimball, C. V., and Marzetta, T. L., 1984, Semblance processing of borehole acoustic array data: Geophysics, **49**, No. 3, 274–281.

Kokesh, F., Schwartz, R., Wall, W., Morris, R. et al., 1965, A new approach to sonic logging and other acoustic measurements: Journal of Petroleum Technology, **17**, No. 03, 282–286.

Li, J., Tao, G., Zhang, K., and Liu, H., 2014a, Acoustic reflection signals extraction by applying blind signal separation, *in* 76th EAGE Conference and Exhibition 2014.

Li, J., Tao, G., Zhang, K., Wang, B., and Wang, H., 2014b, An effective data processing flow for the acoustic reflection image logging: Geophysical Prospecting, **62**, No. 3, 530–539.

Li, Y., Zhou, R., Tang, X., Jackson, J., and Patterson, D., 2002, Single-well imaging with acoustic reflection survey at mounds, oklahoma, usa, *in* 64th EAGE Conference & Exhibition.

Marguerite, L. D. A., 1940, Method of and apparatus for surveying the formations traversed by a bore hole, uS Patent 2,191,119.

Paillet, F., and White, J., 1982, Acoustic modes of propagation in the borehole and their relationship to rock properties: Geophysics, **47**, No. 8, 1215–1228.

Saggaf, M., and Robinson, E. A., 2000, A unified framework for the deconvolution of traces of nonwhite reflectivity: Geophysics, **65**, No. 5, 1660–1676.

Tang, X. M., 2004, Imaging near-borehole structure using directional acoustic-wave measurement: Geophysics, **69**, No. 6, 1378–1386.

Tang, X.-M., and Cheng, C. H. A., 2004, Quantitative borehole acoustic methods, vol. 24: Gulf Professional Publishing.

Tao, G., He, F., Yue, W., and Chen, P., 2008, Processing of array sonic logging data with multi-scale stc technique: Petroleum Science, **5**, No. 3, 238–241.

Yedlin, M. J., Jones, I. F., and Narod, B. B., 1987, Application of the karhunen-loève transform to diffraction separation: Acoustics, Speech and Signal Processing, IEEE Transactions on, **35**, No. 1, 2–8.

Zhang, K., Tao, G., Li, J., Wang, H., Liu, H., and Ye, Q., 2014, 3d fdm modeling of acoustic reflection logging in a deviated well, *in* 76th EAGE Conference and Exhibition 2014.

Zheng, Y., Tang, X. et al., 2005, Imaging near-borehole structure using acoustic logging data with pre-stack fk migration, *in* 2005 SEG Annual Meeting, Society of Exploration Geophysicists.